Photoassociation spectroscopy of a spin-1 Bose-Einstein condensate

C. D. Hamley, E. M. Bookjans, G. Behin-Aein, P. Ahmadi, and M. S. Chapman
School of Physics, Georgia Institute of Technology, Atlanta, Georgia 30332-0430, USA
(Received 20 June 2008; revised manuscript received 5 November 2008; published 2 February 2009)

We report on the high resolution photoassociation spectroscopy of a ^{87}Rb spin-1 Bose-Einstein condensate to the $1_g(P_{3/2})$ $v=152$ excited molecular states. We demonstrate the use of spin dependent photoassociation to experimentally identify the molecular states and their corresponding initial scattering channel. These identifications are in excellent agreement with the eigenvalues of a hyperfine-rotational Hamiltonian. Using the observed spectra we estimate the change in scattering length and identify photoassociation laser light frequency ranges that maximize the change in the spin-dependent mean-field interaction energy.

DOI: 10.1103/PhysRevA.79.023401 PACS number(s): 34.50.Rk, 33.15.Pw

In a spinor Bose-Einstein condensate [1–4], the interplay between different atomic spin orientations results in a small spin dependence of the collisional interaction energy [5]. Though the spin dependence is small relative to the total interaction energy (e.g., ~0.5% in ^{87}Rb), the coherence of the condensate allows observation of unique phenomena such as coherent spin mixing and dynamics [6–10], metastable states [11], spin domains [12,13], and quantum tunneling across spin domains [14]. The spin-dependent interaction energy arises from the small difference in the *s*-wave scattering lengths of the allowed angular momentum channels and manifests in anti- or ferromagnetic properties for a spin-1 condensate, depending on the algebraic sign of the difference. In the two spin-1 condensates investigated to date, ^{23}Na and ^{87}Rb, the former is antiferromagnetic and the latter is ferromagnetic.

Further study of magnetic quantum gases could be greatly aided by the ability to control their magnetic properties. These properties are determined by the *s*-wave scattering lengths, which can be tuned using Feshbach resonances. Both magnetic [15–17] and optical [18–20] Feshbach resonances have been employed to dynamically change these scattering lengths. However, for ^{87}Rb, magnetic Feshbach resonances require large magnetic fields, which suppress spinor dynamics [7,21]. In [22], Jack and Yamashita suggest using multiple photoassociation lines from a vibrational level with a rich hyperfine structure, which would allow parameters that depend on spin dependent scattering lengths to be enhanced between lines from different scattering channels. Specifically, variation of the spin dependent interaction strength could be optimized if there are adjacent molecular states that occur through different scattering channels. In order to identify the existence of such lines, collision channel selective spectroscopy needs to be performed, which requires control over the Zeeman states of the colliding atoms. Note that although the effects of hyperfine levels of the colliding atoms on the photoassociation spectrum has been previously observed [23,24], there has not been any collision channel selective spectroscopy.

In this paper, we report on experimental photoassociation spectroscopy of a spinor condensate. By observing the effect of the Zeeman states of the colliding atoms on the photoassociation spectrum, we extract information about the angular momentum of the molecular states. We identify molecular states that are allowed for a specific scattering channel while forbidden for another. From the spectrum, we calculate the atom loss rate and the expected change in the mean-field interaction energy. Using the observed spectra and these calculations, we identify suitable photoassociation light frequencies that maximize change of the spin dependent interaction strength while minimizing atom loss rates.

The experiment is performed on ^{87}Rb condensates created directly in an optical trap [1]. After a condensate is formed, laser light is used to couple colliding atoms to excited molecular levels, which are subsequently lost from the trap. To measure the spectrum of the molecular excited states, the condensate population losses are measured for different frequencies of the photoassociation (PA) light. The PA excitation laser frequency is tuned near the $1_g(P_{3/2})$ $v=152$ state, which has a rich hyperfine structure and a binding energy of 24.1 cm^{-1} [25,26] below the D_2 line of ^{87}Rb. The PA laser has a focused waist of 80 μm, and its frequency is actively stabilized with an accuracy ~5 MHz using a transfer cavity locked to a stabilized diode laser. Figure 1 shows the observed photoassociation spectrum of the $1_g(P_{3/2})$ $v=152$ state taken using condensates with $|f=1, m_f=-1\rangle$ and $|f=1, m_f=0\rangle$ spin states. A portion of the $|f=1, m_f=-1\rangle$ spectrum was observed in [26]. To avoid mechanical excitation of the condensate, the PA light is ramped up to 3.8 mW in 50 ms, after which it remains on for 100 ms. Successive data points are separated by 5 MHz. The weaker lines identified by $\kappa-\pi$ have been confirmed using higher intensity and longer probe time but are shown here under the same conditions as the stronger lines for consistency. The inset shows a line too weak to be made out in the larger scan. In order to enhance the visibility of this line, the PA light power is increased to 11 mW and left on for 300 ms, and it has been averaged over four scans. For each data point, an absorptive image of the condensate is taken 12 ms after the PA and trapping lasers are turned off. The condensate population is counted and normalized to an average value taken under the same conditions but with the PA light frequency detuned far from any of the molecular lines observed in Fig. 1.

The 1_g potential is categorized as a Hund's case (c) [27]. The relevant good quantum numbers for this potential are total molecular angular momentum F, total nuclear spin I, and Ω, the projection of the rotational angular momentum J on the internuclear axis. For this case $F_{\bar{z}}$, the projection of $\vec{F}$

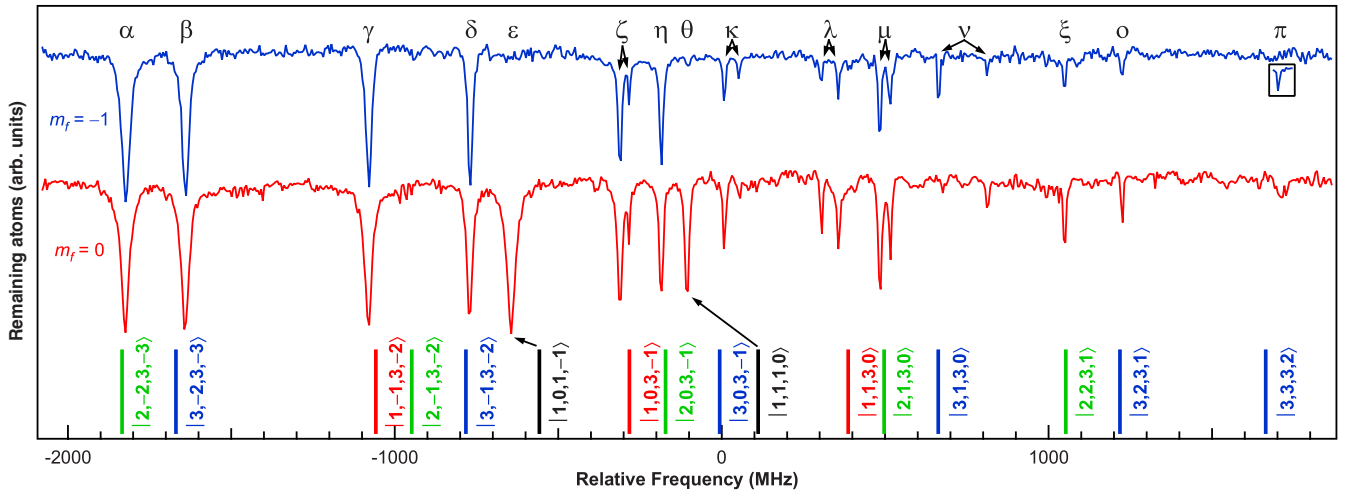

FIG. 1. (Color online) Observed photoassociation spectrum of the $1_g(P_{3/2})$ $v=152$ state for $m_f=-1$ (upper) and $m_f=0$ (lower). These spectra are obtained after 150 ms of exposing a BEC to a PA light with 3.8 mW and 80 μm beam waist. The inset box for $m_f=-1$ is obtained using 350 ms and 11 mW with averaging to enhance visibility of this weaker line. Plots are offset for clarity. The origin of the hyperfine-rotation Hamiltonian fit is used as the zero point for the plot. A stick spectrum with approximate $|F,f,I,i\rangle$ labels is given.

onto the internuclear axis, and $I_{\vec{z}}$, the projection of $\vec{I}$ onto the internuclear axis, are almost good quantum numbers, while J is not [28].

The possible values of F are determined by bosonic symmetry and angular momentum addition rules. For two identical spin-1 bosons, the allowed s-wave collision channels are $F=2$ or 0. Addition of the angular momentum of the colliding atoms and the PA photon specifies the possible total angular momentum F of the available molecular states for each scattering channel. Photoassociation through the total spin-2 scattering channel gives molecular F numbers of 1, 2, and 3 while the total spin 0 scattering channel restricts F to 1 (see Fig. 2).

We use the experimental properties of the photoassociation spectrum to identify these quantum numbers for the observed molecular lines. The most striking difference between the two PA spectra in Fig. 1 is that the lines ε and θ appear only for the condensate containing the $m_f=0$ spin state. Since two $m_f=-1$ atoms can only scatter through the total spin-2 channel, while two $m_f=0$ atoms access both the total spin 2 and 0 channels, this observation indicates that these lines occur through the total spin-0 scattering channel, restricting F for the molecular state represented by these lines to 1. An $m_f=-1$ ($m_f=1$) can only access the total spin-0 scattering channel through collision with an $m_f=1$ ($m_f=-1$) spin state. Therefore if a condensate has a mixture of $m_f=-1$ and $m_f=1$ they should participate in the total spin-0 channel photoassociation, while neither of these spin states should photoassociate on these lines if they coexist in the condensate only with an $m_f=0$ spin state. To illustrate these predictions, PA spectra across the lines ε and θ are taken with condensates containing different mixtures of spin states as shown in Fig. 3.

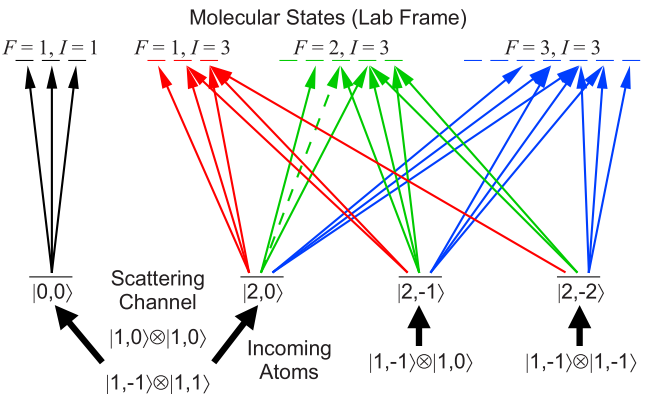

FIG. 2. (Color online) Spin dependent photoassociation. The possible scattering channels of two colliding spin-1 atoms are shown for selected combinations of incoming atoms. Each channel may absorb a PA photon and transit to a bound excited molecular state $|F,M_F\rangle$. All Zeeman projections are in the lab frame relative to a quantization axis defined by an external magnetic field. The $\Delta F=0$, $\Delta M_F=0$ transition indicated by the dashed line is forbidden by the dipole selection rule.

The data shown in Figs. 3(a) and 3(b) are taken with

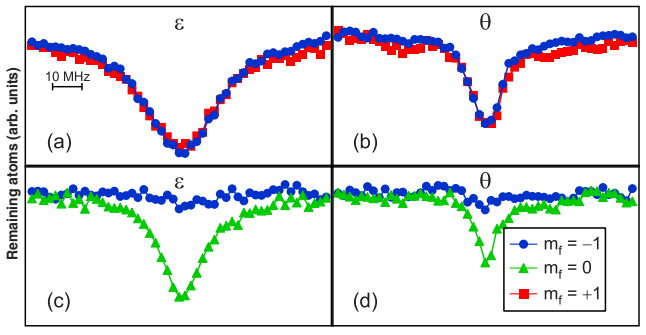

FIG. 3. (Color online) Photoassociation spectroscopy of ε and θ with different mixtures of spin states. (a),(b) Lines ε and θ for mixture of $m_f=-1$ and $m_f=1$ spin states; (c),(d) for mixture of $m_f=-1$ and $m_f=0$. The observed data points corresponding to $m_f=(-1,0,1)$ spin states are represented by circles, triangles, and squares, respectively.

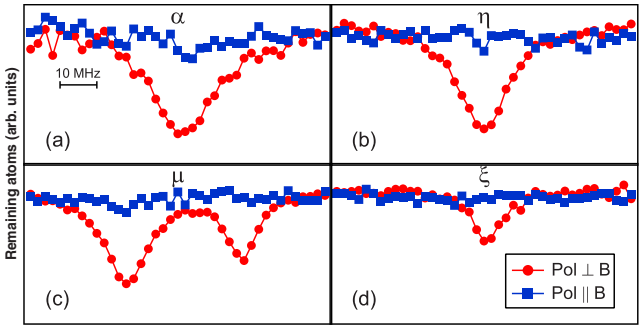

FIG. 4. (Color online) Photoassociation spectroscopy through lines α, η, μ, and ξ for an $m_f=0$ spin state condensate to an $F=2$ molecular state. The data points are taken with the polarization vector of the PA light along (squares) and perpendicular to (circles) an external magnetic field.

similar conditions to Fig. 1, whereas in Figs. 3(c) and 3(d) the photoassociation power is decreased to 1.5 mW to reduce the mechanical effects on the $m_f=-1$ atoms caused by the rapid loss of the $m_f=0$ atoms from the trap. The spin state combinations are prepared using a microwave manipulation technique similar to the one used in Ref. [7]. The populations of different m_f states are counted by spatially separating them using a Stern-Gerlach field during the time of flight. The observed data in this figure show that the $m_f=-1$ and $m_f=1$ spin states participate in the photoassociation for the lines ε and θ if both of them coexist in the condensate, whereas if the $m_f=-1$ spin state coexists with the $m_f=0$ spin state it does not participate in the photoassociation process. This observation matches our analysis based on scattering channels and confirms that $F=1$ for lines ε and θ.

To identify $F=2$ PA lines we note that a $\Delta F=0$, $\Delta M_F=0$ transition from a two-atom collisional spin state $|2, 0\rangle$ to a bound molecular state $|2, 0\rangle$ is forbidden by the electric dipole selection rule as indicated in Fig. 2. Therefore the lines with $F=2$ are suppressed for an $m_f=0$ spin state condensate with π-polarized PA light. Such lines are found by taking a PA spectrum of a pure $m_f=0$ condensate in the presence of an external B field of 1 G along the polarization of the PA light. The observed data for this case, shown in Fig. 4, indicate that the lines α, η, μ, and ξ are absent. By changing the polarization of the PA light perpendicular to the quantization axis defined by the applied B field, all of these lines reappear in the spectrum. A comparison between the observed data with polarization aligned parallel (square) and perpendicular (circle) to the external B field is shown in Fig. 4, which confirms $F=2$ as a good quantum number for these lines. Figure 4(c) also indicates that the line μ is split into two $F=2$ components.

From these observations and the spacing of the lines we are able to assign F and I for the observed lines. This is accomplished by noting that for possible values of $F=1$, 2, and 3 the eigenvalues of $\vec{F}^2$ are 2, 6, and 12. Therefore the separation between molecular states with $F=1$ and 2 should be 2/3 of the frequency separation between the lines with $F=2$ and 3. F numbers for the remaining lines are readily deduced by their spacing and order in each hyperfine grouping. The total nuclear spin for these lines is found by decomposing the initial scattering wave function of the two colliding atoms. This analysis shows that the total nuclear spin must be 1 for the total spin-0 scattering channel and predominantly $I=3$ for the total spin-2 scattering channel. Table I gives the assigned values of F and I for the observed lines.

For the 1_g potential, the molecular hyperfine constant is comparable to the small rotational constant of the state. Therefore the effective Hamiltonian for the 1_g rotation-hyperfine structure can be written as [28]

$$H_{H-R} = a_v \vec{I}\cdot\vec{\Omega} + B_v \vec{J}^2 = a_v I_{\bar{z}}\Omega + B_v\{\vec{F}^2 + \vec{I}^2 - 2F_{\bar{z}}I_{\bar{z}} - \bar{F}_+\bar{I}_- - \bar{F}_-\bar{I}_+\}, \quad (1)$$

where the operators are defined with respect to the internuclear axis $\bar{z}$. A matrix representation of this Hamiltonian is composed of 14 2×2 block diagonal sections and four diagonal states. Since the 2×2 block diagonal sections only mix states with the same values of F and I, the matrix can also be broken up by these quantum numbers. Furthermore, since changing the signs of $F_{\bar{z}}$, $I_{\bar{z}}$, and Ω results in a degenerate state, the states are labeled by F, f, I, and i, where $f=F_{\bar{z}}\Omega$ and $i=I_{\bar{z}}\Omega$. Removing these redundant degeneracies gives matrices for the $I=1$, $F=1$; $I=3$, $F=1$; $I=3$, $F=2$; and $I=3$, $F=3$ which are 2×2; 3×3; 5×5; and 6×6, respectively. The eigenvalues of the Hamiltonian for each combination of F and I are obtained by diagonalizing its corresponding matrix in the $|F,F_{\bar{z}},I,I_{\bar{z}}\rangle$ basis set. The coupling is sufficiently weak that labeling the final states by the almost good quantum numbers of f and i is justified. Figure 5 shows the Hamiltonian matrix broken up by the F and I quantum numbers. The diagonal elements are connected by arrows to their corresponding eigenvalues in the stick spectrum, which are labeled by the basis states. These eigenvalues are fit to the observed spectrum of the $m_f=-1$ condensate of Fig. 1 using the least squares approach. Fitting parameters a_v, B_v, and the frequency offset ω_{offset} are used in the 13 equations generated by setting the diagonalization of the $I=3$ matrices shown in Fig. 5 equal to the energies in the spectrum. In the case of split lines, the stronger one is used for fitting. The least squares fit of these equations specifies a_v and B_v to be 667(5) and 27.6(1.3) MHz, respectively. The positions of the result-

TABLE I. Assigned total angular momentum and nuclear spin of the molecular states appearing in the PA spectra of Fig. 1.

	α	β	γ	δ	ε	ζ	η	θ	κ	λ	μ	ν	ξ	o	π
F	2	3	1	3	1	1	2	1	3	1	2	3	2	3	3
I	3	3	3	3	1	3	3	1	3	3	3	3	3	3	3

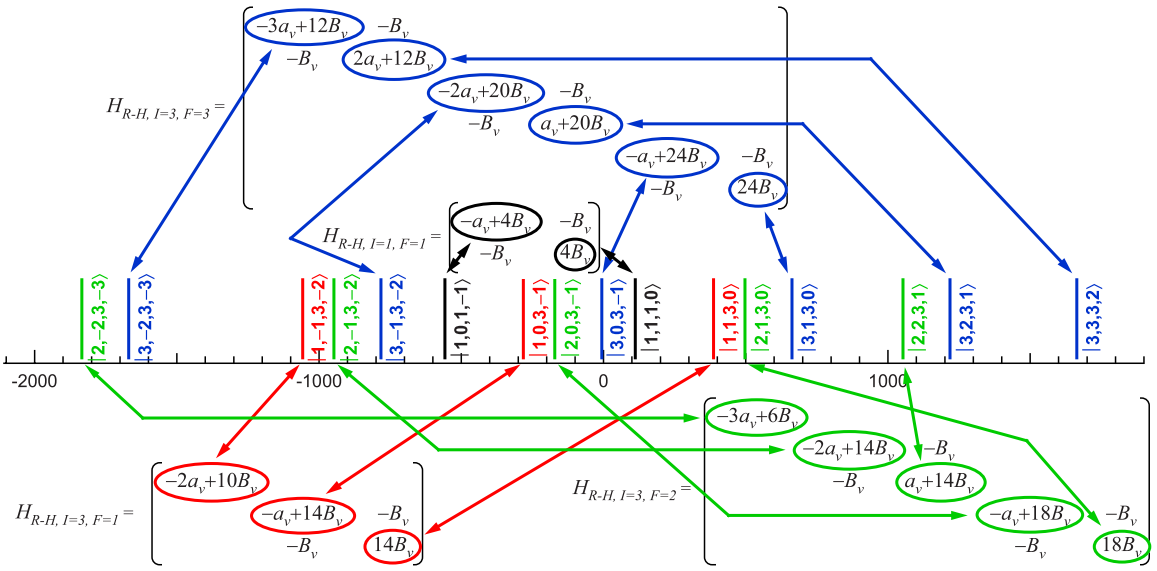

FIG. 5. (Color online) The hyperfine-rotation Hamiltonian is composed of seven 2×2 block diagonal elements and two states which do not mix. Here the sections of the matrix are sorted by the quantum numbers F and I. The diagonal elements are connected to their approximate eigenvalues by arrows. The eigenvalues in the spectrum are labeled by the $|F,f,I,i\rangle$ basis states of the Hamiltonian.

ing eigenvalues are shown as a stick spectrum in Fig. 1, which produces good agreement with the observed lines in the PA spectrum. The stick spectrum is labeled according to the dominant part of the corresponding eigenvectors, which is in agreement with the assigned quantum numbers in Table I.

A few general comments should be made for the observed as well as predicted spectra. First, the molecular state corresponding to the $|2,-1,3,-2\rangle$ eigenstate is not observed under any experimental condition. This line is also absent in a scan of the $v=153$ vibrational level. Second, predicted locations of the lines ε and θ corresponding to the $a_{F=0}$ scattering channel are in poorer agreement with their observed locations compared to the other lines. These two lines are connected by arrows to their assumed eigenvalues in Fig. 1. The separation of these lines is not simply a_v as the Hamiltonian indicates. Also the origin of the Hamiltonian for these lines appears to be different than for the $a_{F=2}$ lines. It is unclear as to whether different fit parameters or a revision to the Hamiltonian is needed to correct these deviations. Last, we note that some of the lines appear to be split on the order of 30–160 MHz. These split lines are connected to their labels in Fig. 1 for clarity. The Hamiltonian presented in Eq. (1) predicts that all lines should be doubly degenerate and does not account for this splitting. This points to an additional interaction not considered in this simple model. These discrepancies are important for refinement of the molecular potential theory.

One of our motivations for studying this system is to assess the suitability of multiple nearby optical Feshbach resonances to manipulate spin dependent properties of a condensate. In an $f=1$ spinor condensate, the magnetic properties are determined by the difference of the s-wave scattering lengths, $\Delta a=a_{F=2}-a_{F=0}$. The magnitude of Δa is proportional to the rate of spin changing collisions while its sign signifies whether the overall behavior is ferromagnetic or antiferromagnetic ($-$ or $+$, respectively). To determine the change in Δa due to the photoassociation light, the observed data from Fig. 1 are fitted to a theoretical formula for the inelastic loss rate (K_{inel}) in order to find the width and amplitude for each line as discussed in Ref. [20]. These fit parameters, along with the condensate density (n_0) and the measured field-free value for Δa of $-1.45(32)$ a_B [7], are then used to calculate the estimated change in Δa as shown in Fig. 7(a).

In order to determine Δa from the spectrum, we make a few simplifying assumptions. For a given line, we assume that the effect on its associated scattering channel can be reduced to merely the measured photoassociation spectrum of the line. PA laser polarization has not produced an observable effect apart from suppressing the forbidden $|2,0\rangle \rightarrow |2,0\rangle$ transition used to identify the $F=2$ molecular states. Since each line can comprise both π and σ transitions to the molecular states, this observation implies that the net effect of polarization is minimal. This can be understood by noting that the lab and molecular frames rarely coincide. Therefore a given transition can see a definite polarization in one frame but mixed polarization in the other one. The polarization significantly affects the photoassociation rate only if the transition is forbidden in one of the frames. It is therefore assumed that the measured line shapes for an $m_f=0$ condensate are sufficient to determine their effects on the associated scattering channel.

To calculate Δa from the spectrum, the data are fit to theoretical equations describing the fractional atom number in terms of the condensate density, pulse time, and the inelastic scattering rate. Since the rate depends on density, which lowers as the condensate is depleted, it is necessary to relate the fraction of remaining atoms to the inelastic scattering rate by the equation [26,29]

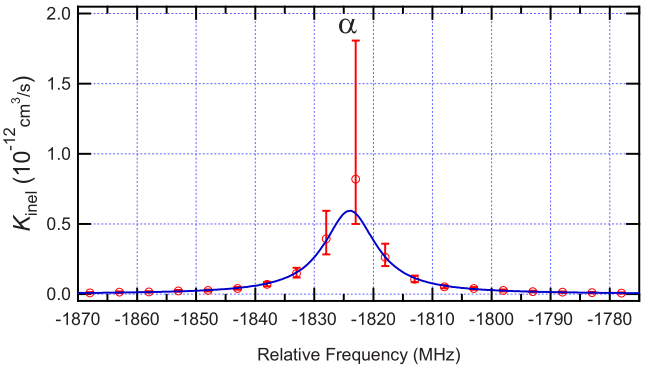

FIG. 6. (Color online) Sample of data fitting for K_{inel}. Circles: Plot of the solution to Eq. (2) for the data on line α with error bars using estimated counting error of 5%. Solid: Plot of Eq. (3) where the weighted least squares fit values are $A=1.59\times10^{-12}$ cm^3, $\Gamma_{spon}=10.7$ MHz, and $\omega_{offset}=-1824$ MHz.

$$\frac{N(\eta)}{N(0)} = \frac{15}{2}\eta^{-5/2} \times \left[\eta^{1/2} + \frac{1}{3}\eta^{3/2} - (1+\eta)^{1/2}\tanh^{-1}\sqrt{\eta/(1+\eta)}\right], \tag{2}$$

where $\eta=2K_{inel}n_0t$. By solving Eq. (2) for each point of the spectrum, we derive K_{inel} as a function of PA laser frequency. We assume a condensate peak density, $n_0=10^{14}$ cm^{-3}, which is typical for our system. To estimate the error of this solution, Eq. (2) is also solved for the data point plus and minus the estimated counting error of 5%. This solution and the corresponding error bars are shown in Fig. 6. The error bars for the points with the smallest fraction of atoms remaining are quite large. Because of this large error in the central points, a weighted fit is used for K_{inel}. Weights are determined by the inverse of the variance, which is approximated by squaring the 5% errors. This technique weights the points in the wings of the Lorentzian more heavily than the center. The data are fit for each line in the spectrum to determine parameters for calculating the change in Δa, where the following equations for a single line are used [20]:

$$K_{inel} = \frac{2\pi\hbar}{m}\frac{1}{k_i}\frac{\Gamma_{stim}\Gamma_{spon}}{\Delta^2 + (\Gamma_{spon}/2)^2}, \tag{3}$$

$$a = a_{bg} + \frac{1}{2k_i}\frac{\Gamma_{stim}\Delta}{\Delta^2 + (\Gamma_{spon}/2)^2}. \tag{4}$$

The parameter k_i is the wave number of the atoms in the condensate. These equations already assume that $\Gamma_{stim} \ll \Gamma_{spon}$ and thus that the PA intensity contributes negligibly to the linewidths. The data for each line's K_{inel} are fit with Γ_{spon}, ω_{offset} ($\Delta=\omega_{PA}-\omega_{offset}$), and $A=\frac{2\pi\hbar}{m}\frac{1}{k_i}\Gamma_{stim}$ used as fitting parameters. A sample fit result for line α is shown in Fig. 6, which demonstrates a good overlap between the fit and the calculated values of K_{inel}. In the following analysis we will use the values of K_{inel} deduced from this fitting technique instead of simply calculating K_{inel} from the observed data, since the fit is considered more reliable.

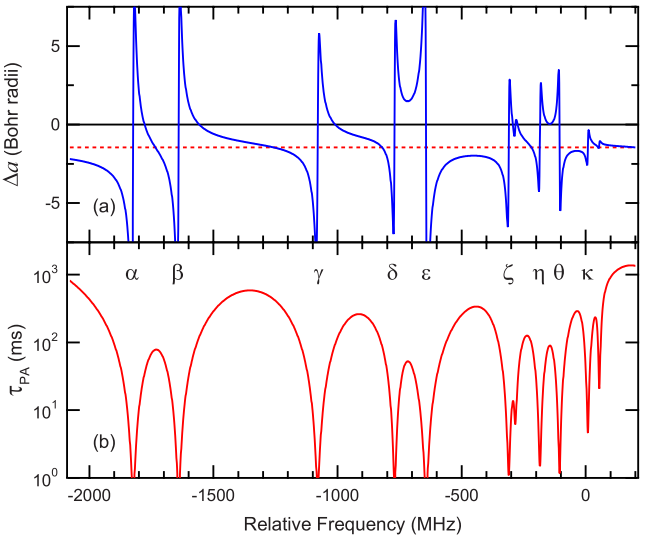

FIG. 7. (Color online) Calculated values for Δa and for the PA limited half-life of the BEC. The dotted line in (a) is the nominal value of Δa, which is −1.45(32) Bohr radii for ^{87}Rb [7]. The intensity here is 33 times that used to take the spectra in Fig. 1.

To obtain the total effect on K_{inel} and on Δa, we assume that for each scattering channel the effects of the PA laser can be calculated by summing the contributions from each photoassociation feature associated with the channel. The total effect on a given channel's scattering length and the total inelastic scattering rate for both channels is given by

$$a_F(\omega_{PA}) = a_{bg,F} + \sum_i \frac{m}{4\pi\hbar}A_{F,i}\frac{\omega_{PA}-\omega_{offset,F,i}}{(\omega_{PA}-\omega_{offset,F,i})^2 + (\Gamma_{spon,F,i}/2)^2}, \tag{5}$$

$$K_{inel}(\omega_{PA}) = \sum_{F,i} A_{F,i}\frac{\Gamma_{spon,F,i}}{(\omega_{PA}-\omega_{offset,F,i})^2 + (\Gamma_{spon,F,i}/2)^2}. \tag{6}$$

Controlling the magnetic properties of ^{87}Rb condensates has three potential goals: changing the interaction from ferromagnetic to antiferromagnetic, reducing the spinor interaction to zero, and increasing the strength of the ferromagnetic interaction. Figure 7 shows the calculated values for making the condensate antiferromagnetic. In Fig. 7, Δa and the photoassociation induced loss-limited half-life, $\tau_{PA}=(K_{inel}n_0)^{-1}$, are plotted for different detunings for a PA intensity of 1250 W/cm^2, which is 33 times higher than used in our experiments. The photoassociation limited lifetime is the time during which spin dependent dynamics can be observed before the condensate is depleted by the photoassociation driven atom loss. With respect to changing the sign of Δa and hence the magnetic nature of the condensate, one of the more promising frequency ranges is between lines δ and ε, which are associated with different scattering channels. Here the influences of the two lines reinforce each other producing a large positive change in Δa. In this region, as the intensity of the PA light increases, the atom loss rate increases con-

tinuously, while $|\Delta a|$ initially lowers to zero and then raises on the antiferromagnetic side. At ≈33 times the spectroscopy intensity, spinor dynamics occur at the same rate as the nominal value of $2\pi \times 4.3(3)$ rad/s [7], but with opposite sign. The PA limited half-life between lines δ and ε for this intensity is 50 ms. While 50 ms is a short half-life, the ratio of the spinor dynamical time to the PA limited half-life is ≈1.3 rad/half-life which is marginally sufficient to observe the effect.

The goal of reducing the spinor dynamical rate to zero can also be accomplished in this region. With an intensity ≈17 times the spectroscopy intensity, Δa goes to zero with a half-life of 100 ms. Regions a few 100 MHz to the blue of the $a_{F=2}$ lines are also promising for reducing Δa to zero with good lifetimes. To enhance the ferromagnetic nature of the condensate, the region between lines ε and ζ is promising. These lines are also from different scattering channels, but in the opposite order. Here the dynamical rate can be doubled with an intensity of 90 times the spectroscopic value, while maintaining a PA limited half-life of 100 ms.

In principle it is possible to produce these effects simply by detuning 1–2 GHz to the blue or red of the entire vibrational level, while increasing the intensity. However, this is challenging for several reasons. First, the laser power needed exceeds several watts which is a few thousand times the spectroscopic power. Second, at these detunings and intensities, other molecular states become important. Between the 1_g, 0_g^-, and 0_u^+ symmetries, resonant features can be found approximately every 10 GHz. Finally, the tensor light shift, which causes an effect similar to magnetic fields, is expected to be significant at these intensities [30,31]. Even at the lower intensities proposed above, the effects of the tensor light shift warrants further study.

In conclusion, we have performed photoassociation spectroscopy on a spin-1 condensate. The spin dependent photoassociation spectrum was used to identify good quantum numbers for some of the molecular states, which are in agreement with theoretical predictions of a hyperfine-rotation Hamiltonian. The results of this study provide a valuable test case to answer general questions about how to model molecular potentials in the presence of hyperfine and rotation interactions. A high resolution photoassociation study of other vibrational levels will provide a deeper understanding of molecular potentials.

The spectrum is also used to predict the photoassociation limited lifetime and change in Δa. It is shown that optical Feshbach resonances to a molecular state with hyperfine structure can be used to alter the spin dependent mean-field interaction energy to change the spinor dynamics of the condensate with limited viability. From the calculations shown in Fig. 7, it is clear that Δa can be altered significantly, while having sufficient PA limited lifetimes needed to see the change in spinor dynamics. However, in order to change the sign of Δa and hence the magnetic nature of the condensate requires intensities and PA frequencies that correspond to challengingly short lifetimes compared to the time needed for spinor dynamics. Also, further investigation of the tensor light shift and techniques to reduce it are needed to implement this scheme.

This work was supported by National Science Foundation Grant No. PHYS-0605049. We would like to thank Tom Bergeman and Eite Tiesinga for helpful discussions.

[1] M. D. Barrett, J. A. Sauer, and M. S. Chapman, Phys. Rev. Lett. **87**, 010404 (2001).
[2] E. A. Cornell, D. S. Hall, M. R. Matthews, and C. E. Wieman, J. Low Temp. Phys. **113**, 151 (1998).
[3] C. J. Myatt, E. A. Burt, R. W. Ghrist, E. A. Cornell, and C. E. Wieman, Phys. Rev. Lett. **78**, 586 (1997).
[4] D. M. Stamper-Kurn, M. R. Andrews, A. P. Chikkatur, S. Inouye, H.-J. Miesner, J. Stenger, and W. Ketterle, Phys. Rev. Lett. **80**, 2027 (1998).
[5] T. L. Ho, Phys. Rev. Lett. **81**, 742 (1998).
[6] M.-S. Chang, C. D. Hamley, M. D. Barrett, J. A. Sauer, K. M. Fortier, W. Zhang, L. You, and M. S. Chapman, Phys. Rev. Lett. **92**, 140403 (2004).
[7] M. S. Chang, Q. Qin, W. Zhang, L. You, and M. S. Chapman, Nat. Phys. **1**, 111 (2005).
[8] W. X. Zhang, D. L. Zhou, M.-S. Chang, M. S. Chapman, and L. You, Phys. Rev. A **72**, 013602 (2005).
[9] H. Schmaljohann, M. Erhard, J. Kronjäger, M. Kottke, S. van Staa, L. Cacciapuoti, J. J. Arlt, K. Bongs, and K. Sengstock, Phys. Rev. Lett. **92**, 040402 (2004).
[10] A. Widera, F. Gerbier, S. Fölling, T. Gericke, O. Mandel, and I. Bloch, Phys. Rev. Lett. **95**, 190405 (2005).
[11] H.-J. Miesner, D. M. Stamper-Kurn, J. Stenger, S. Inouye, A. P. Chikkatur, and W. Ketterle, Phys. Rev. Lett. **82**, 2228 (1999).
[12] J. Stenger, S. Inouye, D. M. Stamper-Kurn, H.-J. Miesner, A. P. Chikkatur, and W. Ketterle, Nature (London) **396**, 345 (1998).
[13] L. E. Sadler, J. M. Higbie, S. R. Leslie, M. Vengalattore, and D. M. Stamper-Kurn, Nature (London) **443**, 312 (2006).
[14] D. M. Stamper-Kurn, H.-J. Miesner, A. P. Chikkatur, S. Inouye, J. Stenger, and W. Ketterle, Phys. Rev. Lett. **83**, 661 (1999).
[15] E. Tiesinga, B. J. Verhaar, and H. T. C. Stoof, Phys. Rev. A **47**, 4114 (1993).
[16] S. Inouye, M. R. Andrews, J. Stenger, H.-J. Miesner, D. M. Stamper-Kurn, and W. Ketterle, Nature (London) **392**, 151 (1998).
[17] S. L. Cornish, N. R. Claussen, J. L. Roberts, E. A. Cornell, and C. E. Wieman, Phys. Rev. Lett. **85**, 1795 (2000).
[18] J. L. Bohn and P. S. Julienne, Phys. Rev. A **56**, 1486 (1997).
[19] F. K. Fatemi, K. M. Jones, and P. D. Lett, Phys. Rev. Lett. **85**, 4462 (2000).
[20] M. Theis, G. Thalhammer, K. Winkler, M. Hellwig, G. Ruff, R. Grimm, and J. H. Denschlag, Phys. Rev. Lett. **93**, 123001 (2004).
[21] H. Schmaljohann, M. Erhard, J. Kronjäger, K. Sengstock, and K. Bongs, Appl. Phys. B: Lasers Opt. **79**, 1001 (2004).

[22] M. W. Jack and M. Yamashita, Phys. Rev. A **71**, 033619 (2005).
[23] E. R. I. Abraham, W. I. McAlexander, H. T. C. Stoof, and R. G. Hulet, Phys. Rev. A **53**, 3092 (1996).
[24] E. Tiesinga, K. M. Jones, P. D. Lett, U. Volz, C. J. Williams, and P. S. Julienne, Phys. Rev. A **71**, 052703 (2005).
[25] J. D. Miller, R. A. Cline, and D. J. Heinzen, Phys. Rev. Lett. **71**, 2204 (1993).
[26] M. Theis, Ph.D. thesis, University of Innsbruck, Innsbruck, 2005.
[27] K. M. Jones, E. Tiesinga, P. D. Lett, and P. S. Julienne, Rev. Mod. Phys. **78**, 483 (2006).
[28] X. Wang, H. Wang, P. L. Gould, W. C. Stwalley, E. Tiesinga, and P. S. Julienne, Phys. Rev. A **57**, 4600 (1998).
[29] C. McKenzie, J. Hecker Denschlag, H. Häffner, A. Browaeys, L. E. E. de Araujo, F. K. Fatemi, K. M. Jones, J. E. Simsarian, D. Cho, A. Simoni, E. Tiesinga, P. S. Julienne, K. Helmerson, P. D. Lett, S. L. Rolston, and W. D. Phillips, Phys. Rev. Lett. **88**, 120403 (2002).
[30] R. Grimm, M. Weidemüller, and Y. B. Ovchinnikov, Adv. At., Mol., Opt. Phys. **42**, 95 (2000).
[31] M. V. Romalis and E. N. Fortson, Phys. Rev. A **59**, 4547 (1999).